



HAL
open science

Giant tunnel-electron injection in nitrogen-doped graphene

Jérôme Lagoute, Frédéric Joucken, Vincent Repain, Yann Tison, Cyril Chacon, Amandine Bellec, Yann Girard, Robert Sporken, Edward H. Conrad, Francois Ducastelle, et al.

► **To cite this version:**

Jérôme Lagoute, Frédéric Joucken, Vincent Repain, Yann Tison, Cyril Chacon, et al.. Giant tunnel-electron injection in nitrogen-doped graphene. *Physical Review B: Condensed Matter and Materials Physics* (1998-2015), 2015, 91, pp.125442. 10.1103/PhysRevB.91.125442 . hal-01445703

HAL Id: hal-01445703

<https://hal.science/hal-01445703>

Submitted on 5 Mar 2024

HAL is a multi-disciplinary open access archive for the deposit and dissemination of scientific research documents, whether they are published or not. The documents may come from teaching and research institutions in France or abroad, or from public or private research centers.

L'archive ouverte pluridisciplinaire **HAL**, est destinée au dépôt et à la diffusion de documents scientifiques de niveau recherche, publiés ou non, émanant des établissements d'enseignement et de recherche français ou étrangers, des laboratoires publics ou privés.



CHORUS

This is the accepted manuscript made available via CHORUS. The article has been published as:

Giant tunnel-electron injection in nitrogen-doped graphene

Jérôme Lagoute, Frédéric Joucken, Vincent Repain, Yann Tison, Cyril Chacon, Amandine Bellec, Yann Girard, Robert Sporken, Edward H. Conrad, François Ducastelle, Mattias Palsgaard, Nick Papior Andersen, Mads Brandbyge, and Sylvie Rousset

Phys. Rev. B **91**, 125442 — Published 31 March 2015

DOI: [10.1103/PhysRevB.91.125442](https://doi.org/10.1103/PhysRevB.91.125442)

Giant tunnel electron injection in nitrogen-doped graphene

Jérôme Lagoute,^{1,*} Frédéric Joucken,² Vincent Repain,¹ Yann Tison,^{1,†} Cyril Chacon,¹ Amandine Bellec,¹ Yann Girard,¹ Robert Sporcken,² Edward H. Conrad,³ François Ducastelle,⁴ Mattias Palsgaard,⁵ Nick Papior Andersen,⁵ Mads Brandbyge,⁵ and Sylvie Rousset¹

¹Laboratoire Matériaux et Phénomènes Quantiques,
Université Paris Diderot-Paris 7, Sorbonne Paris Cité, CNRS, UMR 7162,
10, rue A. Domon et L. Duquet, 75205 Paris 13, France

²Research Center in Physics of Matter and Radiation (PMR),

Université de Namur, 61 Rue de Bruxelles, 5000 Namur, Belgium

³The Georgia Institute of Technology, Atlanta, Georgia 30332-0430, USA

⁴Laboratoire d'Etude des Microstructures, ONERA-CNRS, BP 72, 92322 Châtillon Cedex, France

⁵Center for Nanostructured Graphene, Dept. of Micro- and Nanotechnology,
Technical University of Denmark, Ørsted's Plads,
Bldg. 345E, DK-2800 Kongens Lyngby, Denmark

Scanning tunneling microscopy experiments have been performed to measure the local electron injection in nitrogen-doped graphene on SiC(000 $\bar{1}$) and were successfully compared to *ab initio* calculations. In graphene, a gap-like feature is measured around the Fermi level due to a phonon-mediated tunneling channel. At nitrogen sites, this feature vanishes due to an increase of the elastic channel that is allowed because of symmetry breaking induced by the nitrogen atoms. A large conductance enhancement by a factor of up to 500 was measured at the Fermi level by comparing local spectroscopy at nitrogen sites and at carbon sites. Nitrogen doping can therefore be proposed as a way to improve tunnel electron injection in graphene.

PACS numbers: 73.22.Pr, 63.22.Rc, 68.37.Ef

The exploitation of the electronic properties of graphene allows us to envision the development of new electronics based on carbon materials¹⁻³. Due to the particular band structure of graphene, low energy electronic states, driving the current in transport devices, are only available at the large parallel momentum (k_{\parallel}) K and K' points in graphene. As a consequence, perpendicular tunneling of electrons into a graphene sheet is quenched at low bias voltage due to the competing large k_{\parallel} momentum conservation and the exponentially decaying tunneling probability with increasing k_{\parallel} . Scanning tunneling microscopy (STM) experiments on graphene on SiO₂ have revealed that above 63 mV an inelastic channel corresponding to the excitation of an out-of-plane phonon is opened, which enhances substantially the tunneling current⁴. A gap-like feature in the dI/dV spectroscopy is therefore observed around the Fermi level E_F ⁴⁻⁸. Interestingly, the same feature has been measured in spin devices using magnetic tunnel junctions⁹ where magnetoresistance measurements were performed at bias voltages larger than the gap feature. Using a large bias in such devices can be a limitation as the magnetoresistance signal decreases with the bias voltage. Therefore, enhancing the electron injection at low energy in graphene turns out to be a cornerstone for improving the performances of graphene-based electronic and spintronic devices. As the quenching of electron injection is due to the momentum conservation of electrons imposed by the symmetry of the graphene sheet, breaking the symmetry of the system can lead to an enhancement of electron injection. In that respect, introducing atomic defects is a promising strategy to restore an elastic channel for vertical injection

in graphene. The nitrogen doping of graphene obtained by substitution of nitrogen atoms for carbon atoms is a suitable route to achieve well-controlled and well characterized point defects with limited atomic relaxation⁶⁻⁸ while preserving the band structure of graphene. At the atomic level, nitrogen doping induces a redistribution of the electron density on one sublattice and a localized resonance at nitrogen sites⁸ that have been widely studied theoretically¹⁰. In this Letter, we perform scanning tunneling spectroscopy (STS) experiments to study the local electron injection in nitrogen-doped graphene on SiC(000 $\bar{1}$). dI/dV and tunneling current decay length spectra reveal that below the out-of-plane phonon energy, elastic tunneling is allowed at nitrogen sites leading to a large enhancement of the electron injection by a factor of up to 500 close to zero bias. This interpretation is supported by first principle calculations and well explained by a simple analytical model. Our finding allows us to propose nitrogen doping of graphene as an efficient way to improve electron injection in graphene without altering its band structure.

The graphene sample was grown by the confinement control sublimation (CCS) method on SiC(000 $\bar{1}$)¹¹. It consists of about 5 non-Bernal stacked layers on top of SiC. The post-synthesis doping was achieved in an ultra high vacuum (UHV) chamber by exposing the sample during 30 mn to a nitrogen radical flux produced by a remote (~ 30 cm) RF plasma source (MPD21 from Oxford Applied Research¹²) fed with N₂ (purity 99.999%)⁸. The scanning tunneling experiments were performed with a UHV Low-Temperature STM (4.2 K) from Omicron GmbH using electrochemically-etched tungsten tips.

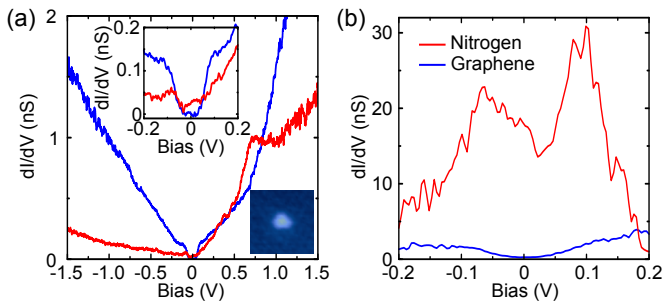


FIG. 1. (a) dI/dV spectra measured above graphene far from the nitrogen atoms (blue) and above a nitrogen atom (red). The spectrum in inset is a zoom at low bias voltages of the spectra. The image in inset is a $2 \times 2 \text{ nm}^2$ image of the nitrogen atom where the measurement was performed. (b) dI/dV spectra around E_F on carbon (blue) and nitrogen (red) sites measured in constant height mode conditions prior to the spectroscopy measurement (110 pA at 100 mV above graphene carbon area).

dI/dV spectra were acquired with a lock-in detector at 710 Hz and a modulation amplitude of 24 mV. Prior to spectroscopic measurement on graphene the STM tip was calibrated on a Au(111) substrate by applying voltage pulses until the dI/dV spectrum shows the onset of the Shockley surface state. This procedure is necessary to obtain reliable spectra as it was mentioned by Y. Zhang et al.⁴. After synthesis and doping, the sample was transported in the atmosphere and outgassed in UHV at $\sim 800^\circ\text{C}$ before the STM measurements.

Nitrogen atoms substituted to carbon atoms (graphitic nitrogen) in graphene on SiC(000 $\bar{1}$) appear in the STM images as bright spots with a triangular shape (right bottom inset in Fig. 1(a)). This can be attributed to a combination of charge transfer between the nitrogen and the three neighbouring carbon atoms⁸ and the opening of the elastic channel as shown in the following. The dI/dV spectrum in Fig. 1(a) measured on graphene far from the nitrogen atoms reveals a gap-like feature of 130 mV around E_F . This feature has been attributed to the inelastic excitation of an out-of-plane phonon⁴. Indeed, momentum conservation in the tunneling process imposes a large in-plane momentum k_{\parallel} for electrons tunneling to graphene where the only available states are at the K points. However, above a threshold voltage corresponding to the energy of an out-of-plane graphene phonon, an inelastic tunneling channel is opened which leads to a large increase of the tunneling current. In the dI/dV spectrum this inelastic excitation appears as two onsets symmetric with respect to E_F at the energy of the phonon. The spectrum measured above a nitrogen atom is totally different (Fig. 1(a)). The inelastic signal almost disappears, only faint onsets can be seen (top inset in Fig. 1(a)). This is indicative of a strong decrease of the inelastic/elastic transmission ratio. A quantitative comparison of the conductance at nitrogen and carbon sites cannot be obtained from the curve in Fig. 1(a) as these

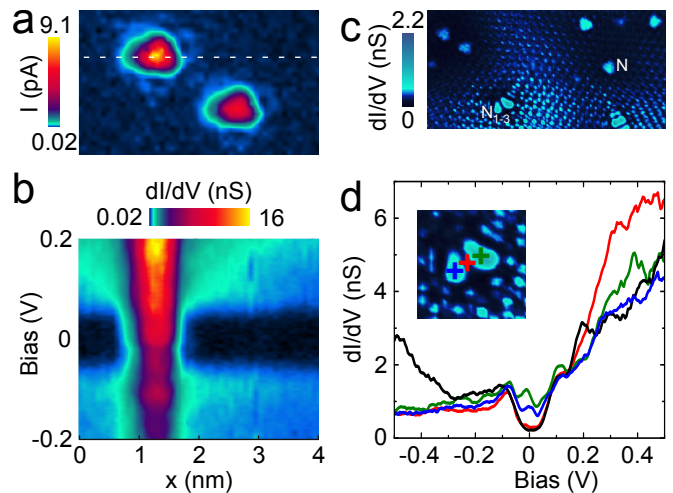


FIG. 2. (a) Current image measured at 1.3 mV in constant height mode ($4 \times 2.4 \text{ nm}^2$, 12 pA at 100 mV above graphene carbon area) on which STS measurements have been performed at each point. (b) 2D map representing the spectra measured along the line shown in (a). (c) Conductance map measured in constant current mode at 2.5 mV ($12 \times 6 \text{ nm}^2$). The marks N and N_{1-3} indicate one single substitutional nitrogen atom, and a nitrogen pair with two nitrogens in second neighbour position. (d) Spectra measured on a pair of nitrogen atoms in second neighbour positions. The black curve was measured on the graphene area far from nitrogen atoms, the color curves were measured at the positions marked by the cross in the inset that is a zoom of (c) corresponding to the nitrogen pair.

spectra were measured with a constant current condition before measurement ($U = 1 \text{ V}, I = 500 \text{ pA}$). Indeed the nitrogen atoms lie in the graphene plane as it was suggested by voltage dependent STM measurements⁸ and confirmed by ab-initio calculations on monolayer¹³ and bilayer^{14,15} graphene. Electronic effects lead to an apparent height of about 1 \AA , the tip-sample distance is larger above the nitrogen atom than above graphene. In order to quantitatively compare the conductance at carbon and nitrogen sites, spectra have to be measured with the same tip-sample distance (constant height mode). Such data are displayed in Fig. 1(b). The measurements obtained with the same tip-sample separation reveal a huge increase of dI/dV above nitrogen. At E_F the conductance at the Fermi level above a nitrogen atom is 70 times larger than on the graphene sheet revealing a very large enhancement of electron injection at nitrogen sites.

The increase of conductance above nitrogen atoms was systematically observed as shown in Fig. 2. Figure 2(a) displays the current image measured in constant height mode on an area with two nitrogen atoms. Figure 2(b) shows the evolution of the spectra along a line crossing a nitrogen atom (cf. dotted line of Fig. 2(a)) revealing the increase of the dI/dV signal above nitrogen over a distance characterized by a full width at half maximum of 5 \AA . This extent corresponds to the typical size of the triangular pattern associated with a nitrogen atom

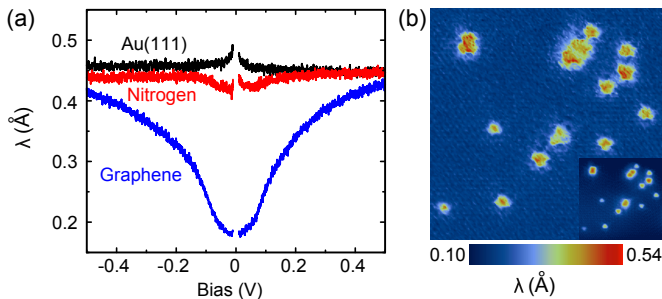


FIG. 3. (a) Voltage dependent current decay length λ measured on a reference Au(111) sample (black), N-doped graphene carbon area (blue) and above a graphitic nitrogen atom in graphene (red). (b) λ mapping at 20 mV extracted from spectra measured at each point of the topographic image shown in the inset ($10 \times 10 \text{ nm}^2$, $U = 0.1 \text{ V}$, $I = 500 \text{ pA}$).

in the STM images. Such a spatial extension also corresponds to the variation of the potential around a nitrogen atom¹⁰. The ratio between the conductance at the Fermi level above graphene (0.017 nS) and above nitrogen (9.15 nS) in Fig. 2 is about 500, which is larger than the above-mentioned measure (ratio of 70). As will be discussed below, we attribute this difference to the tip-sample distance that is larger in the second case, which increases the ratio of conductance between nitrogen and graphene. In Fig. 2(c) we show a conductance map measured in constant current mode at 2.5 mV. Although this mode reduces the contrast, it allows us to obtain more details along the whole image. This image shows again that the conductance is stronger above the nitrogen atoms confirming that the phonon gap feature vanishes above nitrogen as previously observed in the spectrum of Fig. 1(a). Interestingly, on a nitrogen pair identified as two nitrogen atoms in second neighbour positions, a strong contrast with atomic resolution is clearly observed in the dI/dV map. The spectra in Fig. 2(d) measured on the nitrogen atoms and between the nitrogen atoms of this pair clearly reveal that although the inelastic feature is almost suppressed above the nitrogen atoms, it is unaffected at the central position between the N atoms. This is in line with previously reported data showing that the inelastic feature is observed at the center of a nitrogen pair⁷.

Details on the tunneling mechanism at nitrogen sites can be obtained by measuring the voltage dependent current decay length λ as discussed for undoped graphene on SiO_2 ⁴. In that case, the decay length inside and outside the phonon gap has been measured to be 0.25 Å and 0.5 Å respectively⁴ by fitting, at different bias voltages, the $I(z)$ curves with the function $I = \exp(-z/\lambda)$. Here we performed a continuous voltage dependent measure of λ using a lock-in technique. A sinusoidal modulation at 715 Hz with an amplitude of 0.06 Å was applied to the piezo z signal. A lock-in detection was used to record the corresponding current response allowing to measure the dI/dz signal. The measures were performed with a

closed feedback loop in order to keep the current constant during the spectrum and obtain a signal directly proportional to $1/\lambda$. After dividing by the mean value of the current we obtain the $\lambda(V)$ curve. The resulting spectra are shown in Fig. 3(a). The $\lambda(V)$ curve measured above graphene looks similar to previously reported $\lambda(V)$ curves obtained by fitting I versus z measurements⁴. We obtain λ values $\sim 0.18 \text{ Å}$ inside the phonon gap and 0.42 Å outside the phonon gap. As a reference we have measured the $\lambda(V)$ curve on a Au(111) with the same tip just before measuring on the graphene sample. The corresponding curve shows the expected value of 0.45 Å for λ independent of the voltage. Above a nitrogen atom, the $\lambda(V)$ curve obtained is in strong contrast with the one measured on graphene. The $\lambda(V)$ curve above nitrogen is similar to the one measured on Au(111) suggesting that the transport is dominated by elastic tunneling. A slight phonon feature is nevertheless observable with a much weaker amplitude (0.42 Å in the gap, 0.44 Å outside the gap). The use of the lock-in technique allows us to perform a systematic measure of local $\lambda(V)$ spectra at each point of an image and to extract a λ mapping at any bias voltage. An example of such an image is displayed in Fig. 3(b) showing a λ mapping at 20 mV measured simultaneously with the image shown in the inset. This mapping shows a uniform value of λ on the carbon areas of around $\sim 0.2 \text{ Å}$ and a clear larger value on nitrogen atoms of $\sim 0.4 \text{ Å}$. A consequence of the different decreasing lengths at nitrogen and carbon sites is that the conductance ratio between these sites is expected to be distance dependent. Indeed this ratio is expected to increase with the tip-sample distance z according to the quantity $\exp(z(1/\lambda_C - 1/\lambda_N))$ where λ_C and λ_N are the decreasing lengths at E_F above carbon and nitrogen sites respectively. This allows us to understand the different dI/dV ratios measured to be 70 in Fig. 1(b) and 500 in Fig. 2(b). In these measurements, the current above the graphene area at a reference bias of 100 mV is $I_1 = 110 \text{ pA}$ in the Fig. 1(b) and $I_2 = 12 \text{ pA}$ in the Fig. 2(b). This means that the tip-sample distance in the two measurements varies by $\Delta z(V) = \lambda_C(V) \ln(I_1/I_2) = 0.55 \text{ Å}$ (using $\lambda_C(V) = 0.25 \text{ Å}$ for $V = 100 \text{ mV}$). The ratios of conductance are therefore expected to vary by a factor of 5.7 (with $\lambda_C = 0.18 \text{ Å}$ and $\lambda_N = 0.42 \text{ Å}$ at the Fermi level) which is close to the ratio 500/70.

Using the DFT-NEGF method and setup described in^{16,17}, dI/dV spectra including vibrational effects were calculated directly above a nitrogen dopant in graphene and above pristine graphene. For all calculations shown we use a tip-to-sample distance of $d = 5 \text{ Å}$ since tunneling at larger distances is not described well by the LCAO basis set used¹⁸. To simulate single nitrogen sites, the nitrogen atoms were separated by 1.7 nm. To test that this separation was sufficient the STS spectrum was calculated exactly between adjacent nitrogen pairs (8.5 Å away from either site) and seen to coincide with that of pristine graphene. The dI/dV spectra on a nitrogen and pristine graphene are shown in Fig. 4(a). The dotted line shows

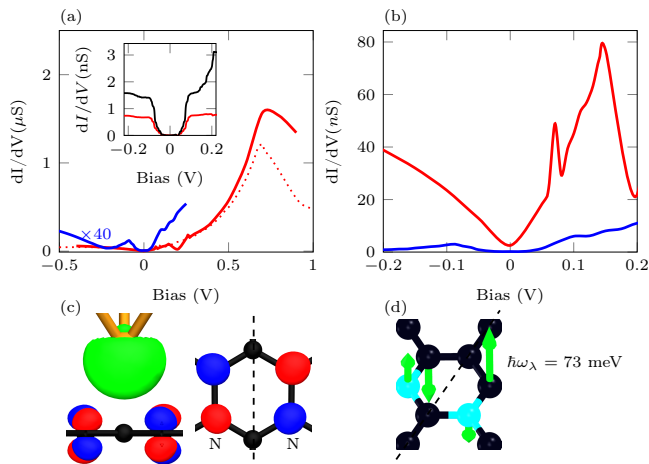


FIG. 4. (a) Calculated dI/dV spectra above pristine graphene (blue) and a nitrogen (red) with (solid) and without (dotted) electron-phonon coupling. The spectrum in inset is a close-up of the inelastic conductance steps near E_F on a single nitrogen (red) and at the center of a nitrogen dimer (black) in graphene. (b) Calculated constant height dI/dV spectra around E_F on pristine graphene (blue) and a nitrogen (red) sites. (c) Resonant scattering state of the nitrogen dimer blue/red indicates positive/negative isovalues. (d) Out-of-plane phonon that mediates tunneling into the scattering state of (c).

the equivalent spectrum above nitrogen without electron-phonon coupling. Note that the spectrum on graphene has been enhanced to allow a better comparison with the experimental data of Fig. 1(a) where the constant current imaging condition brings the intensity of the signal above graphene close to the intensity of the signal above nitrogen. For pristine graphene, the spectrum is dominated by the inelastic features. As discussed previously¹⁶ the 130 meV gap is reproduced, and the dip caused by inelastic tunneling into the Dirac point is seen at the expected bias value. As in the measured dI/dV spectra of Fig. 1(a) a broad resonance emerges at $V_b = 700$ meV above nitrogen, and the inelastic features near the Fermi level are not seen. Comparing the dI/dV spectra above nitrogen with and without electron-phonon coupling, it is clear that the elastic channel dominates, and the inclusion of vibrations only leads to a stronger resonance slightly shifted in bias. In Fig. 4(b) the calculated dI/dV spectra around E_F are shown on the same scale. Comparing these spectra with the constant height measurement of Fig. 1(b), both the conductance magnitudes and their ratio suggest that $d > 5 \text{ \AA}$ in the experiment as expected.

The inelastic steps in dI/dV excluding elastic contributions on nitrogen and at the center of a nitrogen dimer are investigated using the Lowest Order Expansion¹⁹. This method was previously found to give a good description of the gap feature of pristine graphene.¹⁶ The results are shown in the inset of Fig. 4(a). The inelastic steps above a single nitrogen are of similar magnitude to those of pris-

tine graphene, but the elastic contribution is an order of magnitude larger above nitrogen making them nearly invisible in measurements. At the center of the nitrogen dimer the inelastic feature is about 3 times larger. This additional inelastic feature is a result of the mirror symmetry along armchair direction between the two nitrogen sites. The resonant scattering state of the dimer system shown in Fig. 4(c) has odd symmetry at the dimer center and consequently does not couple elastically to the s-like state of the STM-tip. In the presence of the 73 meV out-of-plane phonon shown in Fig. 4(d) the mirror symmetry is broken and a large inelastic step in conductance is seen in very good agreement with the experimental data of Fig. 2(d). Therefore, the DFT-NEGF results support the conclusion based on the measurements that the opening of an elastic channel above nitrogen substitutions leads to a giant increase in tunneling conductance.

The enhancement of the elastic tunnel electron injection at nitrogen sites can be rationalized further in terms of a simple model. In the presence of disorder, k -conservation is broken and an elastic tunneling channel is opened. For the case of N doping the hamiltonian of the system now includes a potential V localized on the impurity sites that produces a resonance about 0.5 eV above the Dirac point in the bulk π states¹⁰. For simplicity we will assume that the free-electron states can be described locally in terms of atomic-like functions. One of them has a π -like character (state of symmetry A_{2u} ²⁰ also denoted 1^- in²¹) and can be coupled to the genuine π states of pristine graphene. Assuming the potential to be localized on the nitrogen atoms, its relevant matrix elements for a single impurity at site 0 only involve the π state at this site $|\pi, 0\rangle$ as well as the localized function associated with the A_{2u} state $|A_{2u}, 0\rangle$. In k -space the potential obviously couples all states. In this very localized limit, the main matrix element $\langle \pi, 0 | V | \pi, 0 \rangle$ has been estimated to be about 10 eV¹⁰. Because of the different extensions of the orbitals the other matrix element should be much weaker, allowing us to keep just one off-diagonal term $v = \langle \pi, 0 | V | A_{2u}, 0 \rangle$. We can now directly adapt the calculation by Wehling et al.²² and calculate the self-energy and the local Green function corresponding to the new Γ elastic channel. Finally, in a second order perturbation theory, the local density of states on the nitrogen site is: $n_\Gamma(E) \simeq v^2 n_\pi(E) / (E - E_\sigma)^2$ where $n_\pi(E)$ is the corresponding density of states of the π states in the presence of the nitrogen impurities¹⁰ and E_σ is the energy of the free-electron like state²².

Close to the Dirac point $E \simeq 0$ and the intensity of the new channel is a fraction $(v/\lambda_{el-ph})^2$ of the inelastic channel, where λ_{el-ph} is the electron phonon coupling strength. Assuming v to be at least equal to λ_{el-ph} (about 0.5 eV²²) we see that the elastic channel can be at least as efficient as the inelastic channel in agreement with the experiments and the above ab initio calculations.

In conclusion, using STM/STS we measured an increase of differential conductance leading to a vanishing of the phonon gap-like feature at nitrogen sites. This

leads to a two orders of magnitude increase in electron injection into graphene. First principle calculations reveal that although the inelastic excitation of graphene phonon still occurs at nitrogen sites, an elastic channel opens that substantially increase the conductance. Therefore we expect that nitrogen doping of graphene can be used to improve tunnel electron injection in graphene-based devices.

I. ACKNOWLEDGMENTS

This work has been supported by the Labex SEAM program No. ANR-11-LABX-86 in the framework of the Program No. ANR-11-IDEX-0005-02. The research leading to these results has received funding from the European Union Seventh Framework Programme under grant agreement no 604391 Graphene Flagship. V.R. thanks the Institut Universitaire de France for support. E. H. C. acknowledges support by the National Science Foundation under Grant DMR-1005880.

* jerome.lagoute@univ-paris-diderot.fr

† New address: Université de Pau et des Pays de l'Adour, IPREM - ECP CNRS UMR 5254, Hélioparc Pau-Pyrénées, 2 av. du Président Angot, 64053 Pau Cedex 9, France

¹ C. Berger, Z. Song, T. Li, X. Li, A. Y. Ogbazghi, R. Feng, Z. Dai, A. N. Marchenkov, E. H. Conrad, P. N. First, and W. A. de Heer, *J. Phys. Chem. B* **108**, 19912 (2004).

² K. S. Novoselov, A. K. Geim, S. V. Morozov, D. Jiang, Y. Zhang, S. V. Dubonos, I. V. Grigorieva, and A. A. Firsov, *Science* **306**, 666 (2004).

³ A. H. Castro Neto, F. Guinea, N. M. R. Peres, K. S. Novoselov, and A. K. Geim, *Reviews of Modern Physics* **81**, 109 (2009).

⁴ Y. Zhang, V. W. Brar, F. Wang, C. Girit, Y. Yayon, M. Panlasigui, A. Zettl, and M. F. Crommie, *Nature Physics* **4**, 627 (2008).

⁵ R. Decker, Y. Wang, V. W. Brar, W. Regan, H.-Z. Tsai, Q. Wu, W. Gannett, A. Zettl, and M. F. Crommie, *Nano Letters* **11**, 2291 (2011).

⁶ L. Zhao, R. He, K. T. Rim, T. Schiros, K. S. Kim, H. Zhou, C. Gutiérrez, S. P. Chockalingam, C. J. Arguello, L. Plov, D. Nordlund, M. S. Hybertsen, D. R. Reichman, T. F. Heinz, P. Kim, A. Pinczuk, G. W. Flynn, and A. N. Papatheopoulos, *Science* **333**, 999 (2011).

⁷ R. Lv, Q. Li, A. R. Botello-Mendez, T. Hayashi, B. Wang, A. Berkdemir, Q. Hao, A. L. Elias, R. Cruz-Silva, H. R. Gutierrez, Y. A. Kim, H. Muramatsu, J. Zhu, M. Endo, H. Terrones, J.-C. Charlier, M. Pan, and M. Terrones, *Scientific Reports* **2**, 586 (2012).

⁸ F. Joucken, Y. Tison, J. Lagoute, J. Dumont, D. Cabosart, B. Zheng, V. Repain, C. Chacon, Y. Girard, A. R. Botello-Méndez, S. Rousset, R. Sporcken, J.-C. Charlier, and L. Henrard, *Physical Review B* **85**, 161408 (2012).

⁹ B. Dlubak, M.-B. Martin, R. S. Weatherup, H. Yang, C. Deranlot, R. Blume, R. Schloegl, A. Fert, A. Anane,

S. Hofmann, P. Seneor, and J. Robertson, *ACS Nano* **6**, 10930 (2012).

¹⁰ P. Lambin, H. Amara, F. Ducastelle, and L. Henrard, *Physical Review B* **86**, 045448 (2012).

¹¹ W. A. de Heer, C. Berger, M. Ruan, M. Sprinkle, X. Li, Y. Hu, B. Zhang, J. Hankinson, and E. Conrad, *Proceedings of the National Academy of Sciences of the United States of America* **108**, 16900 (2011).

¹² R. P. Vaudo, Z. Yu, J. W. Cook, and J. F. Schetzina, *Optics Letters* **18**, 1843 (1993).

¹³ B. Zheng, P. Hermet, and L. Henrard, *ACS Nano* **4**, 4165 (2010).

¹⁴ S.-O. Guillaume, B. Zheng, J.-C. Charlier, and L. Henrard, *Physical Review B* **85**, 035444 (2012).

¹⁵ Luc Henrard, private communication.

¹⁶ M. L. N. Palsgaard, N. P. Andersen, and M. Brandbyge, *arXiv:1410.3001* (2014).

¹⁷ We use a split DZP basis set, a mesh cutoff of 200 Ry, a Monkhorst-Pack k -point mesh of 1x2x1 and the Ceperley-Alder LDA functional²³ functional to calculate the electronic structure. Supercell dimension and k_y of $27 \times 12.8\text{\AA}(101)/27 \times 17\text{\AA}(81)$ is used to calculate inelastic transport for Pristine/Nitrogen doped graphene.

¹⁸ A. Garcia-Lekue and L. W. Wang, *Phys. Rev. B* **82**, 035410 (2010).

¹⁹ J.-T. Lü, R. B. Christensen, G. Foti, T. Frederiksen, T. Gunst, and M. Brandbyge, *Phys. Rev. B* **89**, 081405 (2014).

²⁰ E. Kogan, V. U. Nazarov, V. M. Silkin, and M. Kaveh, *Physical Review B* **89**, 165430 (2014).

²¹ V. M. Silkin, J. Zhao, F. Guinea, E. V. Chulkov, P. M. Echenique, and H. Petek, *Physical Review B* **80**, 121408 (2009).

²² T. O. Wehling, I. Grigorenko, A. I. Lichtenstein, and A. V. Balatsky, *Physical Review Letters* **101**, 216803 (2008).

²³ J. P. Perdew and A. Zunger, *Phys. Rev. B* **23**, 5048 (1981).